Physics-Informed Implicit Representations of Equilibrium Network Flows

Kevin D. Smith* **Francesco Seccamonte*** **Ananthram Swami†** **Francesco Bullo***

Abstract

Flow networks are ubiquitous in natural and engineered systems, and in order to understand and manage these networks, one must quantify the flow of commodities across their edges. This paper considers the estimation problem of predicting unlabeled edge flows from nodal supply and demand. We propose an implicit neural network layer that incorporates two fundamental physical laws: conservation of mass, and the existence of a constitutive relationship between edge flows and nodal states (e.g., Ohm's law). Computing the edge flows from these two laws is a nonlinear inverse problem, which our layer solves efficiently with a specialized contraction mapping. Using implicit differentiation to compute the solution's gradients, our model is able to learn the constitutive relationship within a semi-supervised framework. We demonstrate that our approach can accurately predict edge flows in AC power networks and water distribution systems.

1 Introduction

Network flows are a fundamental aspect of modern society, from traffic and communication networks to power and water distribution systems. Many critical infrastructures are well-modeled as graphs, with edges that transport vital commodities [1]. Beyond infrastructure, network flows are also central to models in epidemiology, ecology, medicine, and chemical networks. Their dynamics have been well-studied in compartmental systems theory [2]. Given the prevalence of flow networks in natural and engineered systems, predicting flows in these networks is an important learning task that may facilitate monitoring, control, optimization, and protection of these networks.

While domain-specific tools to predict network flows have been around for a while, the machine learning community has only recently taken an interest in general-purpose models for network flows. [3] predicts edge flows from partial measurements by making a smoothing assumption, i.e., by minimizing nodal flow divergence. [4] improves on this approach by adding a trainable regularizer that can incorporate side information. Both of these approaches are centered on a notion of approximate conservation, i.e., that the net inflow to each node should be near zero. Since conservation of mass is a universal constraint on network flows, imposing this conservation law is an important step toward embedding physics into the model.

But the conservation law alone is not enough to uniquely determine flow, which is why both [3] and [4] rely on heuristic regularizers to select the "best" conservation-respecting flow. In fact, physical networks are often governed by a *pair* of physical laws: the conservation law, and a *constitutive relationship*, which specifies the magnitude and direction of each edge flow based on "effort" variables at each incident node (e.g., pressure or voltage). For example, in DC circuits, currents are conserved according to Kirchoff's current law, and Ohm's law is the constitutive relationship that relates current flows to nodal potentials. The conservation law and the constitutive relationship together define the unique edge flows (and nodal efforts).

*Center for Control, Dynamical Systems, and Computation, University of California, Santa Barbara, CA 93106 USA, {kevinsmith, fseccamonte, bullo}@ucsb.edu

†U.S. Army Research Laboratory, Adelphi, MD 20783 USA

36th Conference on Neural Information Processing Systems (NeurIPS 2022).

1.1 Contributions

This paper proposes a model for network flows that embeds both the conservation law and existence of a constitutive relationship. Our model, which we call an *Implicit Flow Network* (IFN), predicts each edge flow using a trainable nonlinear function of latent nodal variables. These latent variables are constrained to a manifold wherein the conservation law is satisfied. In addition to introducing IFN, we offer the following contributions: (i) a contraction algorithm that is able to both evaluate the IFN layer and backpropagate gradients through it, (ii) an explicit upper bound on the number of iterations required by this algorithm, (iii) a rigorous theoretical comparison between IFN and the state-of-the-art flow estimation methods in [3, 4], and (iv) numerical experiments from several AC power networks and water distribution systems that indicate IFN can significantly outperform these baselines on the flow estimation task. Additionally, because IFN requires a nonlinearity with a constrained slope, we provide (v) a novel "derivative-constrained perceptron", which is essentially a trainable activation function with upper and lower bounds on its slope.

1.2 Related Work

Network Flow Estimation Flows on graphs are a classical topic in computer science [5], and flow forecasting has long been studied in specific domains like traffic [6], but interest in the flow estimation task from a machine learning perspective appears to be relatively recent. Deep learning algorithms have been used to predict traffic flows [7, 8] and power flows [9], but [3] and [4] appear to be the first papers to propose methods for domain-agnostic flow prediction, based on the notion of divergence minimization.

Implicit Neural Networks IFN belongs to a growing class of models called implicit neural networks, which do not explicitly state the output of the model; rather, they describe a desired relationship between the model's inputs and outputs. In the prevailing implicit framework, the output is defined as a fixed point of a trainable perceptron. This approach was introduced in [10] as a "deep equilibrium network". Subsequent work has developed new frameworks for ensuring the existence of the fixed point and computing it [11, 12, 13, 14, 15]. Other types of implicit neural networks include neural ODEs [16] and layers that solve convex optimization problems [17] and Nash equilibria [18].

Graph Neural Networks Graph neural networks (GNN) are a diverse family of models for network-related learning tasks that incorporate graph structure directly into the model. GNNs can typically be classified into three types, in increasing order of generality [19, §5.3]: convolutional models [20, 21], attentional models [22], and message-passing models [23, 24]. Recently, [25] proposed an implicit graph convolutional network. Analogously, IFN can be interpreted as an implicit message-passing GNN, with flows serving as messages and latent nodal variables acting as an embedding.

1.3 Preliminaries and Notation

Given a directed graph $G = (\mathcal{V}, \mathcal{E})$, the signed incidence matrix $B \in \{-1, 0, 1\}^{|\mathcal{V}| \times |\mathcal{E}|}$ is the matrix with entries

$$B_{i,e} = \begin{cases} 1, & i \text{ is the head of } e \\ -1, & i \text{ is the tail of } e \\ 0, & \text{else} \end{cases}, \quad \forall i \in \mathcal{V} \text{ and } e \in \mathcal{E}$$

For an undirected graph, the signed incidence matrix is obtained by assigning an aribtrary orientation to each edge. For each $i \in \mathcal{V}$, let $\mathcal{N}_{\text{in}}(i), \mathcal{N}_{\text{out}}(i) \subset \mathcal{V}$ be the in-neighbors and out-neighbors of i.

Given a vector $x \in \mathbb{R}^n$, we use the notation $[x]$ to denote the diagonal matrix $\text{diag}(x) \in \mathbb{R}^{n \times n}$. Where such notation would be unclear (e.g., may be confused with brackets to indicate order of operations), we fall back on the $\text{diag}(\cdot)$ notation. We write $x^\perp$ to refer to the vector space that is orthogonal to x, i.e., the space $\{x' \in \mathbb{R}^n : x^\top x' = 0\}$. Given a positive definite diagonal matrix $D \in \mathbb{R}^{n \times n}$, we write $||x||_{2,D}$ to represent the weighted 2-norm $||D^{\frac{1}{2}} x||_2$. Given any matrix M, M_i is the ith column vector of M, and $M^{(j)}$ is the transpose of the jth row vector.

Flow	Nodal Variable	$h(y) =$
DC Current	Voltage	y
DC Power	Voltage	y^2
AC Power (lossless)	Voltage Angle	$\sin(y)$
Water Flow Rate	Hydraulic Head	$\text{sign}(y)\lvert y\rvert^{0.54}$
Mechanical Force Networks	Position	y

Table 1: Examples of physical flow networks and their constitutive relationships.

2 Implicit Flow Networks

IFN is inspired by the physics of network systems. In many physical networks, nodes "communicate" through the exchange of a commodity, like power, water, or force, which can be represented as edge flows. Flows obey a conservation law: for all $i \in \mathcal{V}$,

$$0 = \overbrace{u_i + \sum_{j \in \mathcal{N}_{\text{in}}(i)} f_{(i,j)}}^{\text{net inflow}} - \overbrace{\sum_{j' \in \mathcal{N}_{\text{out}}(i)} f_{(i,j')}}^{\text{net outflow}}, \tag{1}$$

where $u \in \mathbb{R}^{|\mathcal{V}|}$ are nodal inflows from outside the network, and $f \in \mathbb{R}^{|\mathcal{E}|}$ are the edge flows. Furthermore, the flows are related to nodal variables through a constitutive relationship (CR); there is some strictly increasing function h such that, for all $(i,j) \in \mathcal{E}$,

$$f_{(i,j)} = a_{(i,j)} h(x_i - x_j), \tag{2}$$

where $a \in \mathbb{R}^{|\mathcal{E}|}$ are edge weights and $x \in \mathbb{R}^{|\mathcal{V}|}$ are nodal "efforts" or "potentials." For example, in DC power networks, the CR is Ohm's law $f_{(i,j)} = r_{(i,j)}^{-1}(x_i - x_j)$, where r are resistances and x are voltages. In lossless AC networks, the CR is the active power flow equation $f_{(i,j)} = a_{(i,j)} \sin(x_i - x_j)$, where the edge weights are a function of line parameters and x are voltage angles [26, §6.4]. In water distribution systems, the CR is the Hazen-Williams formula [27, Sec. 8.15]. Table 1 lists several flow networks, the physical interpretation of the effort variables x, and the flow function h.

We propose IFN as a layer that predicts edge flows based on these two physical laws—conservation and the existence of a CR:

Definition 2.1 (Implicit Flow Network)**.** An *implicit flow network* (IFN) is a module with the following components:

1. fixed parameters $0 < d_{\min} \leq d_{\max}$,
2. trainable parameters $\theta \in \mathbb{R}^r$ for some r, and
3. a family of differentiable functions $h_\theta : \mathbb{R} \to \mathbb{R}$ such that $d_{\min} \leq h'_\theta(y) \leq d_{\max}$ for all $y \in \mathbb{R}$ and $\theta \in \mathbb{R}^r$, which we call *flow functions*.

The module requires each of the following inputs:

1. a weighted, connected, undirected graph $G = (\mathcal{V}, \mathcal{E}, a)$ with edge weights $a \in \mathbb{R}_{>0}^{|\mathcal{E}|}$, and
2. a supply / demand vector $u \in \mathbb{R}^{|\mathcal{V}|}$ such that $\sum_{i \in \mathcal{V}} u_i = 0$.

The module outputs the unique vector $f \in \mathbb{R}^{|\mathcal{E}|}$ for which there exists $x \in \mathbb{R}^{|\mathcal{V}|}$ such that

$$Bf = u \tag{3}$$

$$f = [a] h_\theta(B^\top x) \tag{4}$$

where $B \in \{-1, 0, 1\}^{|\mathcal{V}| \times |\mathcal{E}|}$ is the signed incidence matrix of G, and h_θ is applied element-wise. We use the notation $\text{FN}_{h,\theta}(G, u)$ to represent the solution f given inputs G and u, flow functions h, and parameters θ.

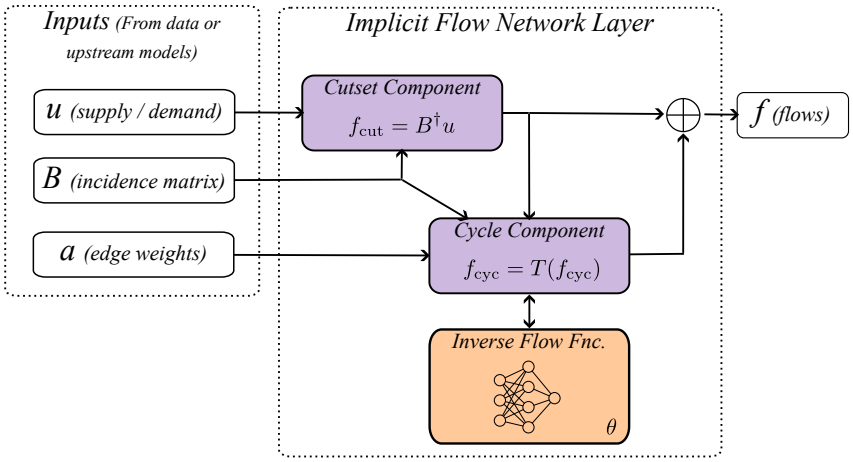

Figure 1: Diagram of the IFN. Inputs are the supply / demand vector u, incidence matrix B, and edges weights a, which are either known or output from upstream models. The IFN layer separately computes the cutset component and cycle component of the flows, with a trainable model for the inverse of the flow function in the CR. These components are summed and output as the flow prediction, for downstream use.

We will prove that IFNs are well-posed in Theorem 2.2. Note that (3) and (4) are just vectorized statements of the conservation law (1) and the CR (2), so these two physical laws directly define the output. The IFN's only trainable component is its flow function, parameterized by θ. In practice, we will only make calls to the *inverse* of the flow function when evaluating and backpropagating through IFN layers, so it is convenient to learn the inverse flow function directly.

We emphasize that IFNs are layers that can be situated in more complex architectures, with other models upstream estimating the supply / demand vector, edge weights, or even the topology. For example, in power systems, demand forecasting is a very well-studied problem [28, 29], and one can solve the economic dispatch problem to forecast power generation at each node [30], collectively leading to an estimate of the supply / demand vector.

2.1 Evaluating the Implicit Flow Network

Our approach to evaluating the implicit flow network is adapted from [31] and is illustrated in Figure 1. Any undirected graph G induces a direct decomposition of the edge flow space $\mathbb{R}^{|\mathcal{E}|}$: given the incidence matrix $B \in \{-1, 0, 1\}^{|\mathcal{V}|\times|\mathcal{E}|}$, the *cycle space* $\ker(B)$ and *cutset space* $\mathrm{Img}(B^\top)$ are orthogonal, and $\mathbb{R}^{|\mathcal{E}|} = \ker(B) \oplus \mathrm{Img}(B^\top)$. We refer the reader to [32, §9.4] for a primer on cycle and cutset spaces. Accordingly, we decompose the vector $f = \mathrm{FN}_{h,\theta}(G, u)$ as $f = f_{\text{cyc}} + f_{\text{cut}}$, where $f_{\text{cyc}} \in \ker(B)$ and $f_{\text{cut}} \in \mathrm{Img}(B^\top)$. The cutset component is readily determined from (3), since $Bf = Bf_{\text{cut}} = u$ implies that $f_{\text{cut}} = B^\dagger u$. Then we must analyze (4) to solve for f_{cyc}. Define a *cycle projection matrix* $P \in \mathbb{R}^{m\times m}$ as the oblique projection onto $\ker(B)$ parallel to $\mathrm{Img}([a]B^\top)$:

$$P = I_m - [a]B^\top \left(B[a]B^\top\right)^\dagger B \tag{5}$$

Based on this projection, we define a map $T : \ker(B) \to \ker(B)$ for all $f_{\text{cyc}} \in \ker(B)$ by

$$T(f_{\text{cyc}}) = P\left(f_{\text{cyc}} - d_{\min}[a]h_\theta^{-1}([a]^{-1}f_{\text{cyc}} + [a]^{-1}B^\dagger u)\right) \tag{6}$$

We can show that f_{cyc} is the unique fixed point of T, and that T is a contraction mapping, leading to a simple algorithm to compute this fixed point.

Theorem 2.2 (Properties of T)**.** *Consider an implicit flow network with parameters $d_{\min}$, $d_{\max}$, and θ, with flow functions h_θ. Suppose that the inputs $G = (\mathcal{V}, \mathcal{E}, a)$ and $u \in \mathbb{1}_{|\mathcal{V}|}^\perp$ are given, and let $B \in \{-1, 0, 1\}^{|\mathcal{V}|\times|\mathcal{E}|}$ be the signed incidence matrix of G. The following are true:*

1. *T is a contraction mapping with respect to $||\cdot||_{2,[a]^{-1}}$, with Lipschitz constant*

$$\mathrm{Lip}(T) \le 1 - \frac{d_{\min}}{d_{\max}},$$

2. *the sequence of iterates* $f_{\text{cyc}}^{(k+1)} = T(f_{\text{cyc}}^{(k)})$ *starting from any initial condition* $f_{\text{cyc}}^{(0)} \in \ker(B)$ *converges to a unique fixed point* f_{cyc}*,*

3. *the output of the implicit flow network is unique and given by*

$$\text{FN}_{h,\theta}(G, u) = f_{\text{cyc}} + B^{\dagger} u \tag{7}$$

Consequently, IFN is well-posed.

Theorem 2.2 provides a simple algorithm for computing the IFN output f: pick any $f_{\text{cyc}}^{(0)} \in \ker(B)$, repeatedly apply the map T until approximate convergence, then add $B^{\dagger}u$. Some care is required when implementing this map. Since P is a dense matrix with $|\mathcal{E}|^2$ entries, it is undesirable to explicitly construct the cycle space projection matrix for large networks. Instead, in order to project a vector $v \in \mathbb{R}^{|\mathcal{E}|}$, we can use the fact that

$$w \triangleq (B[a]B^{\top})^{\dagger} Bv = \underset{w \in \mathbb{R}^n}{\text{argmin}} \left\{ ||B[a]B^{\top}w - Bv||_2 \right\}$$

so the projection is evaluated as $Pv = v - [a]B^{\top}w$. Using this method of projection to implement T, the fixed point iteration to compute $\text{FN}_{h,\theta}(G, u)$ is stated in Algorithm 1.

Algorithm 1 Evaluating the implicit flow network.

1: $B \leftarrow$ signed incidence matrix of G
2: $f_{\text{cut}} \leftarrow \text{argmin}_{f_{\text{cut}} \in \mathbb{R}^m} \{||Bf_{\text{cut}} - u||_2\}$
3: $f_{\text{cyc}} \leftarrow \mathbb{0}_m$
4: $\Delta f_{\text{cyc}} \leftarrow \infty \mathbb{1}_m$
5: **while** $||\Delta f_{\text{cyc}}||_{2,[a]^{-1}} > \epsilon$ **do**
6: $\quad v \leftarrow d_{\min}[a]h_{\theta}^{-1}\left([a]^{-1}f_{\text{cyc}} + [a]^{-1}f_{\text{cut}}\right)$
7: $\quad w \leftarrow \text{argmin}_{w \in \mathbb{R}^n} \left\{||B[a]B^{\top}w - Bv||_2\right\}$
8: $\quad \Delta f_{\text{cyc}} \leftarrow v - [a]B^{\top}w$
9: $\quad f_{\text{cyc}} \leftarrow f_{\text{cyc}} - \Delta f_{\text{cyc}}$
10: **end while**
11: $f \leftarrow f_{\text{cyc}} + f_{\text{cut}}$
12: **return** f

Theorem 2.3 (Implicit Flow Networks, Forward Pass)**.** *Consider an implicit flow network with parameters* $d_{\min}$*,* $d_{\max}$*, and* θ*, with flow functions* h_{θ}*. Suppose that the inputs* $G = (\mathcal{V}, \mathcal{E}, a)$ *and* $u \in \mathbb{1}_{|\mathcal{V}|}^{\perp}$ *are given, and let* $B \in \{-1, 0, 1\}^{|\mathcal{V}| \times |\mathcal{E}|}$ *be the signed incidence matrix of* G*. The following are true of Algorithm 1, with a tolerance of* $\epsilon > 0$*:*

1. *for each iteration* $k = 1, 2, \ldots$ *of the loop, let* $f_{\text{cyc}}^{(k)}$ *represent the new value of* f_{cyc} *defined on line 9; and let* $f_{\text{cyc}}^{(0)} = \mathbb{0}_m$*. Then*

$$f_{\text{cyc}}^{(k+1)} = T(f_{\text{cyc}}^{(k)}), \quad \forall k \geq 0;$$

2. *the algorithm converges with at most* k^* *iterations of the while loop, where*

$$k^* = 1 + \frac{\log\left(d_{\min}^{-1}\rho^{-1}\epsilon\right)}{\log\left(1 - \frac{d_{\min}}{d_{\max}}\right)} \tag{8}$$

and $\rho = ||[a]^{\frac{1}{2}}h_{\theta}^{-1}([a]^{-1}B^{\dagger}u)||_2$*; and*

3. *the algorithm returns* $f \in \mathbb{R}^{|\mathcal{E}|}$*, where*

$$||f - \text{FN}_{h,\theta}(G, u)||_{2,[a]^{-1}} \leq \left(\frac{d_{\max} - d_{\min}}{d_{\min}}\right)\epsilon \tag{9}$$

If evaluating h_{θ}^{-1} is sufficiently simple, then the most expensive step in the iteration is solving the ordinary least squares problem on line 7. Using a general-purpose solver, the complexity of this

operation is roughly $O(|\mathcal{V}|^3)$. But $B[a]B^\top$ is a sparse Laplacian matrix, so we can use a specialized Laplacian solver that reduces the complexity to $O(|\mathcal{E}| \log^k |\mathcal{E}|)$ for some constant k [33].

The bound on the number of iterations k^* can be computed before any forward pass, since evaluating h_θ^{-1} does not require solving the IFN equations. But we can further simplify the bound by approximating $h_\theta^{-1}(0) = 0$, which is often justified because physical flow functions generally have a root at the origin. Using the fact that $(h_\theta^{-1})'(y) \leq d_{\min}^{-1} y$, we can then eliminate the dependence on h_θ^{-1}:

$$k^* \leq 1 + \log\left(1 - \frac{d_{\min}}{d_{\max}}\right)\left(\log \epsilon - \log\left(||[a]^{-\frac{1}{2}} B^\dagger u||_2\right)\right)$$

2.2 Computing the Gradients

In order to train the flow function and any upstream models, it is necessary to backpropagate gradients through the IFN layer. We can perform this backward pass using implicit differentiation, and it turns out that the gradients of $\mathrm{FN}_{h,\theta}(G, u)$ with respect to the parameters θ, a, and u can also be computed using Algorithm 1, i.e., by writing the gradient as the output of an auxiliary implicit flow network.

Theorem 2.4 (Gradients)**.** *Consider an implicit flow network with parameters $d_{\min}$, $d_{\max}$, and θ, with flow functions h_θ. Suppose that the inputs $G = (\mathcal{V}, \mathcal{E}, a)$ and $u \in \mathbb{1}_{|\mathcal{V}|}^\perp$ are given, and let $B \in \{-1, 0, 1\}^{|\mathcal{V}| \times |\mathcal{E}|}$ be the signed incidence matrix of G. Let $f = \mathrm{FN}_{h,\theta}(G, u)$, and let w be a scalar entry of θ, a, or u. We can compute the derivatives $\frac{df}{dw}$ as follows.*

Define a vector of flow functions $g : \mathbb{R}^{|\mathcal{E}|} \to \mathbb{R}^{|\mathcal{E}|}$ by

$$g(\eta) = \mathcal{D}^{-1}\left(\eta - [a]^{-1}\frac{\partial v}{\partial w}\right), \quad \forall \eta \in \mathbb{R}^{|\mathcal{E}|} \tag{10}$$

where $\mathcal{D} \in \mathbb{R}^{|\mathcal{E}| \times |\mathcal{E}|}$ is the diagonal matrix with entries

$$\mathcal{D}_{ee} = \left.\frac{dh_\theta^{-1}(y_e)}{dy_e}\right|_{y_e = a_e^{-1} f_e}, \quad \forall e \in \mathcal{E} \tag{11}$$

and $v = [a]h_\theta^{-1}([a]^{-1} f_{\mathrm{cyc}} + [a]^{-1} B^\dagger u)$. Then

$$\frac{df}{dw} = \mathrm{FN}_{g,\cdot}(G, \mathbb{0}_n) + B^\dagger \frac{du}{dw} \tag{12}$$

(We use the notation $\cdot$ in place of θ, since g has no trainable parameters.) Furthermore, the derivative constraint parameters $d_{\min}, d_{\max}$ from the original implicit flow network are valid for the new implicit flow network.

In other words, to compute the gradient with respect to a parameter, we perform a single evaluation of the implicit flow network. In order to compute the derivatives with respect to some parameter or input w, we first evaluate the partial derivatives $\frac{\partial v}{\partial w}$ and the total derivatives $\frac{du}{dw}$. Then we construct the flow functions g according to (10), and solve an implicit flow network to find $\frac{df}{dw}$ according to (12). It is easy to evaluate $\frac{du}{dw}$, but for convenience, we provide the values of $\frac{\partial v}{\partial w}$ below:

$$\frac{\partial v}{\partial \theta_i} = [a]\frac{dh_\theta^{-1}([a]^{-1} f)}{d\theta_i}, \qquad \frac{\partial v}{\partial a_e} = \mathrm{diag}\left(h_\theta^{-1}([a]^{-1} f) - [a]^{-1}\mathcal{D} f\right)_e, \qquad \frac{\partial v}{\partial u_i} = \left(\mathcal{D} B^\dagger\right)_i$$

3 Comparison with Optimization Models

Both of the state-of-the-art methods for flow estimation, from [3] and [4], use an optimization problem to predict flows. After a suitable transformation to incorporate external flow injections u, we can state this optimization problem as

$$\hat{f} = \underset{f \in \mathbb{R}^{|\mathcal{E}|}}{\mathrm{argmin}} \left\{ ||f||_{2,[q]}^2 + \lambda^2 ||Bf - u||_2^2 \text{ s.t. } f_e = \tilde{f}_e, \ \ \forall \text{ labeled edges } e \in \mathcal{E} \right\} \tag{13}$$

where $\lambda > 0$, and $q > \mathbb{0}_m$ is some vector of edge weights. In [3], $q = \mathbb{1}_m$, while [4] allows q to be the output of a neural network. IFN is not explicitly an optimization problem, but it can be cast as one that is similar to (13):

Theorem 3.1 (Optimization Form of IFN)**.** *Consider an IFN with flow function h_θ. Suppose that the inputs $G = (\mathcal{V}, \mathcal{E}, a)$ and $u \in \mathbb{1}_{|\mathcal{V}|}^{\perp}$ are given, and let $B \in \{-1, 0, 1\}^{|\mathcal{V}| \times |\mathcal{E}|}$ be the signed incidence matrix of G. Then the IFN output can be stated as the solution of a convex optimization problem:*

$$\mathrm{FN}_{h,\theta}(G, u) = \underset{f \in \mathbb{R}^m}{\operatorname{argmin}} \left\{ \sum_{e \in \mathcal{E}} \int_0^{f_e} h_\theta^{-1}(a_e^{-1} z)\, dz \text{ s.t. } Bf = u \right\} \tag{14}$$

Theorem 3.1 can be interpreted as a nonlinear generalization of the Thomson principle from electrical circuits theory [34]. Interestingly, the theorem sets up a direct comparison between IFN and the models in [3] and [4]. If the flow function h_θ is the identity map, then (14) can be simplified as

$$\mathrm{FN}_{h,\theta}(G, u) = \underset{f \in \mathbb{R}^m}{\operatorname{argmin}} \left\{ \sum_{e \in \mathcal{E}} ||f||_{2,[a]^{-1}}^2 \text{ s.t. } Bf = u \right\} \tag{15}$$

Ignoring the constraints from labeled flows, we can interpret (13) as using a penalty method to approximate the output of an IFN with a linear flow function. Thus, we have three distinct differences between IFN and the optimization-based approaches. First, IFN allows for a nonlinear flow function, while [3] and [4] implicitly assume a linear CR. Second, IFN imposes flow conservation as a hard constraint rather than an approximate constraint (which is a limitation if u is uncertain). Finally, IFN does not incorporate flow measurements directly; rather, the model exploits these measurements during training to learn the proper flow function (and train any upstream models for the IFN inputs), making it less sensitive to noise in the labeled flows.

4 Models for Flow Functions

In order to implement an IFN, it is necessary to parameterize its inverse flow function h_θ^{-1}. Since the flow function is essentially a trainable activation function, i.e., a scalar nonlinearity, simple models are likely to be sufficient. The main difficulty with selecting a flow function is that its slope must be bounded by $d_{\min} \leq h'_\theta(y) \leq d_{\max}$ for all $y \in \mathbb{R}$. This section proposes a simple scalar nonlinearity that is guaranteed to respect arbitrary upper and lower bounds on its slope.

Definition 4.1 (Derivative-Constrained Perceptron)**.** Let $k \in \mathbb{Z}_{>0}$ be a hidden layer size, let $a, b, c \in \mathbb{R}^k$ be freely trainable parameters (encoded within the parameter vector θ), and let σ be a non-expansive activation. Let $p, q \geq 1$ such that $p^{-1} + q^{-1} = 1$, and let $\bar{d}_{\min} \leq \bar{d}_{\max} \in \mathbb{R}$. Then the *derivative-constrained perceptron* $\mathrm{N}(x, \theta)$ is the 3-layer neural network defined by

$$\bar{c}(\theta) = \left(1 - \frac{(||c||_p ||a||_q - 1)_+}{||c||_p ||a||_q}\right) c \tag{L1}$$

$$\mathrm{N}_0(x, \theta) = \bar{c}^\top(\theta) \sigma(ax + b) \tag{L2}$$

$$\mathrm{N}(x, \theta) = \left(\frac{\bar{d}_{\max} - \bar{d}_{\min}}{2}\right) \mathrm{N}_0(x, \theta) + \left(\frac{\bar{d}_{\max} + \bar{d}_{\min}}{2}\right) x \tag{L3}$$

Intuitively, (L1) re-scales c so that the perceptron in (L2) is guaranteed to be non-expansive in x. Then (L3) re-centers and re-scales the derivatives of the perceptron from the range $[-1, 1]$ to $[\bar{d}_{\min}, \bar{d}_{\max}]$.

Theorem 4.2 (Derivative-Constrained Perceptron)**.** *Let $\mathrm{N}(x, \theta)$ be a derivative-constrained perceptron with $\bar{d}_{\min} \leq \bar{d}_{\max} \in \mathbb{R}$. Then for all parameter values θ,*

$$\bar{d}_{\min} \leq \frac{d}{dx} \mathrm{N}(x, \theta) \leq \bar{d}_{\max}, \quad \forall x \in \mathbb{R} \tag{16}$$

Note that the values $\bar{d}_{\min}, \bar{d}_{\max}$ in Definition 4.1 and Theorem 4.2 are distinct from the IFN parameters $d_{\min}, d_{\max}$. Since we parameterize the *inverse* flow function h_θ^{-1} in IFN, one shoudl set $\bar{d}_{\min} = d_{\max}^{-1}$ and $\bar{d}_{\max} = d_{\min}^{-1}$ to implement h_θ^{-1} with a derivative-constrained perceptron.

5 Numerical Experiments

We studied the transductive task of predicting unlabeled flows, given that some labeled flows in the same network are known. If the edges $\mathcal{E}$ are partitioned into a labeled set $\mathcal{E}_l$ and an unlabeled set $\mathcal{E}_u$,

the task is to predict the missing flows $\{f_e : e \in \mathcal{E}_u\}$ given the labeled flows $\{f_e : e \in \mathcal{E}_l\}$. For each network, we randomly selected a fraction of the edges to be labeled edges, and we trained IFN and baselines on the labeled edges. Then we evaluated the RMSE of the flows predicted for the unlabeled edges $\mathcal{E}_u$ to compute the testing error. See Appendix B in the supplementary material for full details. Code is available at https://github.com/KevinDalySmith/implicit-flow-networks.

5.1 Datasets

AC Power We selected 6 standard power network test cases. The first 4 test cases (IEEE-57, IEEE-118, IEEE-145, and IEEE-300) are synthetic transmission system test cases, while the remaining cases ACTIVSg200 and ACTIVSg500 are similar to the Illinois and South Carolina power grids, respectively [35]. Each test case contains the topology and electrical parameters of the power network, as well as baseline demands and power injections at each node. While branch resistances are typically small, we set them to zero to ensure lossless transmission lines. We used the MATPOWER toolbox [36] to solve the power flow equations, then recorded the active power flows on each branch (f), computed the net active power injections at each node (u), and selected relevant electrical parameters as edge attributes (series reactance, tap ratio, and voltage magnitude at the two incident nodes).

Water Distribution We selected 3 sample water distribution networks from the ASCE Task Committee on Research Databases for Water Distribution Systems database [37], representing municipal water distribution systems in Fairfield, CA, Bellingham, WA, and Harrisburg, PA. Each network contains the topology of the distribution system, as well as the characteristics of pipes and other network elements and nodal demands. We used the WNTR package [38] to compute the flow rates through each pipe (f), net inflow rate at each node (u), and edge weights associated with each pipe.

5.2 Models and Experiment Details

IFN Architecture In order to use the IFN layer to predict power flows, we created a two-layer model. The first layer estimates positive edge weights $a \in \mathbb{R}^{|\mathcal{E}|}$ according to $a_e = \exp(\mathrm{L}(z_e))$ for all $e \in \mathcal{E}$, where L is a linear module, and z_e is the log-transformed vector of edge attributes. The second layer is an IFN. To predict water flows, we used an IFN layer alone, supplying the edge weights from the dataset as input (rather than learning them from other edge attributes). For both water and power, the IFN layer uses a derivative-constrained perceptron as the inverse flow function ($k = 128$, $p = q = \frac{1}{2}$) with a ReLU activation function. For power, we set $d_{\min} = 0.4$ and $d_{\max} = 2$; and for water, $d_{\min} = 0.2$ and $d_{\max} = 20$.

Baselines We compared the IFN model against four baselines. The minimum divergence method (*Div*) from [3] minimizes the nodal divergence $||Bf||_2^2$ and a regularization term $\lambda||f||_2^2$. The bilevel optimization methods from [4] replace the uniform regularizer with a weighted regularizer $||f||_{2,[q]}^2$, where q is a vector of weights. In *Bil-MLP* and *Bil-GCN*, q is the output of either a 2-layer MLP or GCN model with edge attributes as inputs (we use 64 nodes in each hidden layer with ReLU activations). In *Bil-True*, we specify q as the reciprocal of the coefficient in the linearized CR for AC power networks, so that *Bil-True* approximates (15) with a as the ground-truth edge weight. For water experiments, *Bil-True* uses the same edge weights as the IFN model.

All of the baselines assume that nodal divergence Bf should be approximately zero, but nodes in power networks inject and withdraw power according to the supply / demand vector u, resulting in nonzero divergence. Thus, when we evaluate the baselines, we transform the power network into a divergence-free network by introducing a "source node", adding an edge from the source node to all nodes in $\mathcal{V}$, and treating the entries of u as the flows along each corresponding virtual edge.

5.3 Results

Figure 2 reports the results for the AC power networks, and Figure 3 reports the results for water distribution systems. In both types of networks, the IFN model significantly outperforms the baselines on all of the networks when a small fraction of edges are labeled (less than 80% in power and less than 60% in water). While the other baselines tend to improve as more labeled edges are made available for training, IFN achieves near-optimal performance with as few as 10% of the edges labeled.

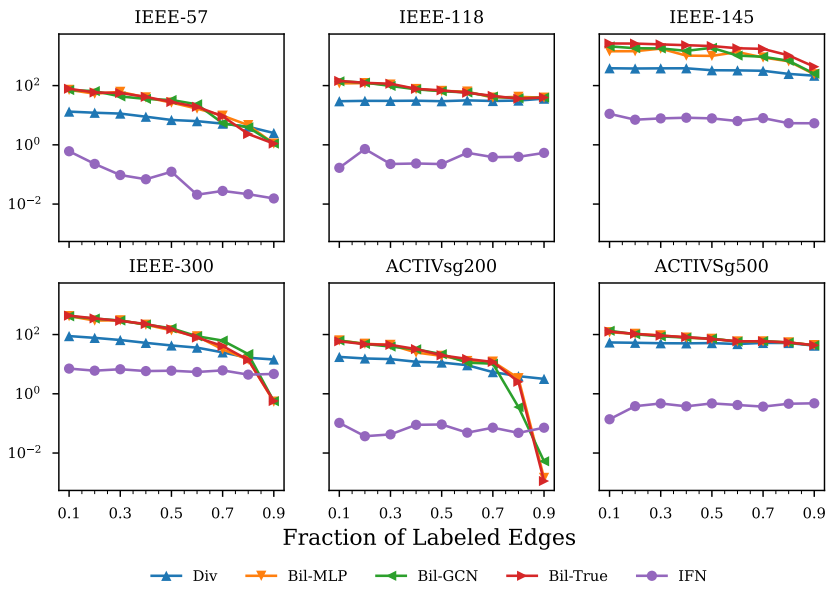

Figure 2: Results for missing flow prediction in AC power networks. Reported values are the RMSE (in units of MW) on the testing set, averaged across 10 trials. Note the vertical axis is in a log scale.

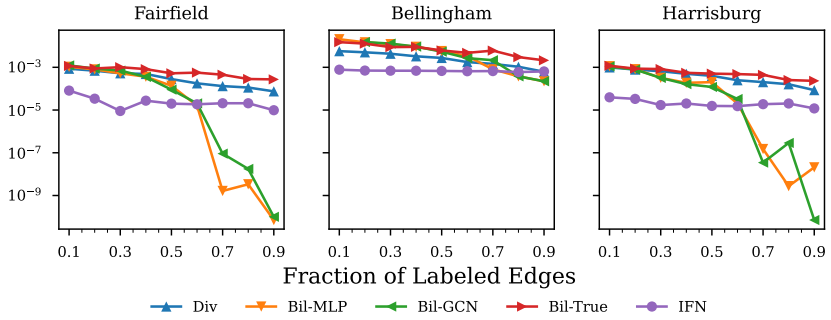

Figure 3: Results for missing flow prediction in water distribution systems. Reported values are the RMSE (in units of m^3/s) on the testing set, averaged across 10 trials.

6 Conclusion

In this paper, we have introduced an implicit model for network flows that incorporates physics through a conservation law and through the existence of a constitutive relationship between flows and nodal variables. We have demonstrated that a simple architecture using this model can learn to accurately predict active power flows in AC networks and water distribution systems. Future work may investigate more elaborate architectures using IFN as a layer, wherein the supply / demand vector, edge weights, or even the graph itself could be predicted from upstream models, and the flows themselves used for downstream tasks. Another interesting extension may be to extend our method to networks with higher-order interactions, i.e., hypergraphs [39] and simplicial complexes [40, 41].

IFN has some limitations that should also be addressed in future work. IFN assumes that the graph is undirected, which does not adequately model networks with unidirectional flows (e.g., traffic) or lossy flows (e.g., resistive power grids). IFN also assumes a CR that depends on the *difference* between nodal variables. This form appears frequently in physical systems, but in other network flow models (like Daganzo traffic models [42]), the CR has a more general dependence on the nodal variables. These limitations may be addressed with extensions of IFN's contraction algorithm.

References

[1] S. M. Rinaldi, J. P. Peerenboom, and T. K. Kelly. Identifying, understanding, and analyzing critical infrastructure interdependencies. *IEEE Control Systems Magazine*, 21(6):11–25, 2001.

[2] J. A. Jacquez and C. P. Simon. Qualitative theory of compartmental systems. *SIAM Review*, 35(1):43–79, 1993.

[3] J. Jia, M. T. Schaub, S. Segarra, and A. R. Benson. Graph-based semi-supervised & active learning for edge flows. In *ACM International Conference on Knowledge Discovery and Data Mining (SIGKDD)*, page 761–771, July 2019.

[4] A. Silva, F. Kocayusufoglu, S. Jafarpour, F. Bullo, A. Swami, and A. K. Singh. Combining physics and machine learning for network flow estimation. In *International Conference on Learning Representations*, Online, May 2021.

[5] L. R. Ford and D. R. Fulkerson. Maximal flow through a network. In *Canadian Journal of Mathematics*, volume 8, pages 399–404, 1956.

[6] M. Lippi, M. Bertini, and P. Frasconi. Short-term traffic flow forecasting: An experimental comparison of time-series analysis and supervised learning. *IEEE Transactions on Intelligent Transportation Systems*, 14(2):871–882, 2013.

[7] Y. Li, R. Yu, C. Shahabi, and Y. Liu. Diffusion convolutional recurrent neural network: Data-driven traffic forecasting. In *International Conference on Learning Representations*, 2018.

[8] H. Yao, X. Tang, H. Wei, G. Zheng, and Z. Li. Revisiting spatial-temporal similarity: A deep learning framework for traffic prediction. In *Proceedings of the AAAI conference on artificial intelligence*, volume 33, pages 5668–5675, 2019.

[9] L. Böttcher, H. Wolf, B. Jung, P. Lutat, M. Trageser, O. Pohl, A. Ulbig, and M. Grohe. Solving AC power flow with graph neural networks under realistic constraints. *arXiv preprint arXiv:2204.07000*, 2022.

[10] S. Bai, J. Z. Kolter, and V. Koltun. Deep equilibrium models. In *Advances in Neural Information Processing Systems*, 2019.

[11] E. Winston and J. Z. Kolter. Monotone operator equilibrium networks. In *Advances in Neural Information Processing Systems*, 2020.

[12] M. Revay, R. Wang, and I. R. Manchester. Lipschitz bounded equilibrium networks. 2020.

[13] L. El Ghaoui, F. Gu, B. Travacca, A. Askari, and A. Tsai. Implicit deep learning. *SIAM Journal on Mathematics of Data Science*, 3(3):930–958, 2021.

[14] S. Jafarpour, A. Davydov, A. V. Proskurnikov, and F. Bullo. Robust implicit networks via non-Euclidean contractions. In *Advances in Neural Information Processing Systems*, December 2021.

[15] S. W. Fung, H. Heaton, Q. Li, D. McKenzie, S. Osher, and W. Yin. Fixed point networks: Implicit depth models with Jacobian-free backprop, 2021. ArXiv e-print.

[16] R. T. Q. Chen, Y. Rubanova, J. Bettencourt, and D. Duvenaud. Neural ordinary differential equations. In *Advances in Neural Information Processing Systems*, 2018.

[17] A. Agrawal, B. Amos, S. Barratt, S. Boyd, S. Diamond, and J. Z. Kolter. Differentiable convex optimization layers. In *Advances in Neural Information Processing Systems*, 2019.

[18] H. Heaton, D. McKenzie, Q. Li, S. W. Fung, S. Osher, and W. Yin. Learn to predict equilibria via fixed point networks. *arXiv preprint arXiv:2106.00906*, 2021.

[19] M. M. Bronstein, J. Bruna, T. Cohen, and P. Veličković. Geometric deep learning: Grids, groups, graphs, geodesics, and gauges. *arXiv preprint arXiv:2104.13478*, 2021.

[20] T. N. Kipf and M. Welling. Semi-supervised classification with graph convolutional networks. *arXiv preprint arXiv:1609.02907*, 2016.

[21] W. Hamilton, Z. Ying, and J. Leskovec. Inductive representation learning on large graphs. *Advances in neural information processing systems*, 30, 2017.

[22] P. Veličković, G. Cucurull, A. Casanova, A. Romero, P. Liò, and Y. Bengio. Graph attention networks. *arXiv preprint arXiv:1710.10903*, 2017.

[23] J. Gilmer, S. S. Schoenholz, P. F. Riley, O. Vinyals, and G. E. Dahl. Neural message passing for quantum chemistry. In *International Conference on Machine Learning*, pages 1263–1272. PMLR, 2017.

[24] P. Battaglia, R. Pascanu, M. Lai, D. Jimenez Rezende, and K. Kavukcuoglu. Interaction networks for learning about objects, relations and physics. In *Advances in Neural Information Processing Systems*. 2016.

[25] F. Gu, H. Chang, W. Zhu, S. Sojoudi, and L. El Ghaoui. Implicit graph neural networks. In *Advances in Neural Information Processing Systems*, 2020.

[26] P. Kundur. *Power System Stability and Control*. McGraw-Hill, 1994.

[27] E. John Finnemore and Joseph B. Franzini. *Fluid mechanics with engineering applications*. McGraw-Hill, tenth edition, 2002.

[28] A. K. Singh, Ibraheem, S. Khatoon, M. Muazzam, and D. K. Chaturvedi. Load forecasting techniques and methodologies: A review. In *2012 2nd International Conference on Power, Control and Embedded Systems*. IEEE, 2012.

[29] G. M. U. Din and A. K. Marnerides. Short term power load forecasting using deep neural networks. In *2017 International conference on computing, networking and communications (ICNC)*, pages 594–598. IEEE, 2017.

[30] K. D. Smith and K. Studarus. Limited-knowledge economic dispatch prediction using bayesian averaging of single-node models. In *2018 IEEE International Conference on Probabilistic Methods Applied to Power Systems (PMAPS)*. IEEE, 2018.

[31] S. Jafarpour, E. Y. Huang, K. D. Smith, and F. Bullo. Flow and elastic networks on the n-torus: Geometry, analysis and computation. *SIAM Review*, 64(1):59–104, 2022.

[32] F. Bullo. *Lectures on Network Systems*. Kindle Direct Publishing, 1.6 edition, January 2022.

[33] N. K. Vishnoi. $Lx = b$, Laplacian solvers and their algorithmic applications. *Theoretical Computer Science*, 8(1-2):1–141, 2013.

[34] P. G. Doyle and J. L. Snell. *Random Walks and Electric Networks*. Mathematical Association of America, 1984.

[35] A. B. Birchfield, T. Xu, K. M. Gegner, K. S. Shetye, and T. J. Overbye. Grid structural characteristics as validation criteria for synthetic networks. *IEEE Transactions on power systems*, 32(4):3258–3265, 2016.

[36] R. D. Zimmerman, C. E. Murillo-Sánchez, and R. J. Thomas. MATPOWER: Steady-state operations, planning, and analysis tools for power systems research and education. *IEEE Transactions on Power Systems*, 26(1):12–19, 2011.

[37] E. Hernadez, S. Hoagland, and L. Ormsbee. Water distribution database for research applications. In *World Environmental and Water Resources Congress*, pages 465–474, 2016.

[38] K. A. Klise, R. Murray, and T. Haxton. An overview of the water network tool for resilience (WNTR). In *Proceedings of the 1st International WDSA/CCWI Joint Conference*, volume 1, 2018.

[39] J. Jo, J. Baek, S. Lee, D. Kim, M. Kang, and S. J. Hwang. Edge representation learning with hypergraphs. In M. Ranzato, A. Beygelzimer, Y. Dauphin, P.S. Liang, and J. Wortman Vaughan, editors, *Advances in Neural Information Processing Systems*, volume 34, pages 7534–7546. Curran Associates, Inc., 2021.

[40] T. Mitchell Roddenberry, Nicholas Glaze, and Santiago Segarra. Principled simplicial neural networks for trajectory prediction. In Marina Meila and Tong Zhang, editors, *Proceedings of the 38th International Conference on Machine Learning*, volume 139 of *Proceedings of Machine Learning Research*, pages 9020–9029. PMLR, 18–24 Jul 2021.

[41] Maosheng Yang, Elvin Isufi, Michael T. Schaub, and Geert Leus. Simplicial convolutional filters. *arXiv prepint arXiv:2201.11720*, 2022.

[42] G. Como. On resilient control of dynamical flow networks. *Annual Reviews in Control*, 43:80–90, 2017.

Checklist

1. For all authors...
   (a) Do the main claims made in the abstract and introduction accurately reflect the paper's contributions and scope? [Yes]
   (b) Did you describe the limitations of your work? [Yes]
   (c) Did you discuss any potential negative societal impacts of your work? [N/A] We do not forsee any negative societal impacts from flow estimation. On the contrary, we hope that these techniques will be useful for managing and protecting critical infrastructure.
   (d) Have you read the ethics review guidelines and ensured that your paper conforms to them? [Yes]
2. If you are including theoretical results...
   (a) Did you state the full set of assumptions of all theoretical results? [Yes]
   (b) Did you include complete proofs of all theoretical results? [Yes]
3. If you ran experiments...
   (a) Did you include the code, data, and instructions needed to reproduce the main experimental results (either in the supplemental material or as a URL)? [Yes] Code and detailed instructions are included in the supplementary material.
   (b) Did you specify all the training details (e.g., data splits, hyperparameters, how they were chosen)? [Yes] Training details are discussed in the supplementary material.
   (c) Did you report error bars (e.g., with respect to the random seed after running experiments multiple times)? [No] While error bars could be included in Figure 2, we felt it added considerable clutter to an already dense plot.
   (d) Did you include the total amount of compute and the type of resources used (e.g., type of GPUs, internal cluster, or cloud provider)? [Yes] As mentioned in Section 5.2, computation was performed in a Google Colab notebook. GPU type varies in Colab, so we did not report the specifics.
4. If you are using existing assets (e.g., code, data, models) or curating/releasing new assets...
   (a) If your work uses existing assets, did you cite the creators? [Yes]
   (b) Did you mention the license of the assets? [No]
   (c) Did you include any new assets either in the supplemental material or as a URL? [Yes]
   (d) Did you discuss whether and how consent was obtained from people whose data you're using/curating? [N/A]
   (e) Did you discuss whether the data you are using/curating contains personally identifiable information or offensive content? [N/A]
5. If you used crowdsourcing or conducted research with human subjects...
   (a) Did you include the full text of instructions given to participants and screenshots, if applicable? [N/A]
   (b) Did you describe any potential participant risks, with links to Institutional Review Board (IRB) approvals, if applicable? [N/A]
   (c) Did you include the estimated hourly wage paid to participants and the total amount spent on participant compensation? [N/A]

A Proofs

A.1 Proof of Theorem 2.2

To prove statement 1, choose any $f_{\text{cyc}} \in \ker(B)$, let $y = [a]^{-1} f_{\text{cyc}} + [a]^{-1} B^{\dagger} u$ for brevity, and observe that

$$\begin{aligned}
\left|\left|\frac{\partial T(f_{\text{cyc}})}{\partial f_{\text{cyc}}}\right|\right|_{2,[a]^{-1}} &= \left|\left|[a]^{-\frac{1}{2}} P \left(I_m - d_{\min}[a] \frac{\partial h_\theta^{-1}(y)}{\partial y} [a]^{-1}\right) [a]^{\frac{1}{2}}\right|\right|_2 \\
&\leq ||[a]^{-\frac{1}{2}} P[a]||_2 \left|\left|[a] \left(I_m - d_{\min}[a] \frac{\partial h_\theta^{-1}(y)}{\partial y} [a]^{-1}\right) [a]^{\frac{1}{2}}\right|\right|_2 \\
&= \left|\left|[a]^{-\frac{1}{2}} \left(I_m - d_{\min}[a] \frac{\partial h_\theta^{-1}(y)}{\partial y} [a]^{-1}[a]^{-1}\right) [a]^{\frac{1}{2}}\right|\right|_2
\end{aligned}$$

where $||[a]^{-\frac{1}{2}} P[a]^{\frac{1}{2}}||_2 = 1$ because $[a]^{-\frac{1}{2}} P[a]^{\frac{1}{2}}$ is a symmetric and idempotent matrix, i.e., an orthogonal projection. Then

$$\left|\left|\frac{\partial T(f_{\text{cyc}})}{\partial f_{\text{cyc}}}\right|\right|_{2,[a]^{-1}} = \max_{e \in \mathcal{E}} \left|1 - d_{\min}(h_\theta^{-1})'(y_e)\right| \leq 1 - \frac{d_{\min}}{d_{\max}}$$

Hence

$$\text{Lip}(T) = \sup_{f_{\text{cyc}} \in \mathbb{R}^m} \left|\left|\frac{\partial T(f_{\text{cyc}})}{\partial f_{\text{cyc}}}\right|\right|_{2,[a]^{-1}} \leq 1 - \frac{d_{\min}}{d_{\max}} < 1$$

Then statement 2 follows from statement 1 and the Banach fixed point theorem. To prove statement 3, observe that $f_{\text{cyc}} = P f_{\text{cyc}}$, so $f_{\text{cyc}} = T(f_{\text{cyc}})$ if and only if

$$P[a] h_\theta^{-1}\left([a]^{-1} f\right) = \mathbb{0}_m \tag{17}$$

where $f = f_{\text{cyc}} + B^{\dagger} u$. But $\ker(P[a]) = \text{Img}(B^\top)$, so (17) is equivalent to the existence of $x \in \mathbb{R}^n$ such that

$$h^{-1}([a]^{-1} f) = B^\top x \tag{18}$$

and (18) is equivalent to (4).

A.2 Proof of Theorem 2.3

To prove statement 1, let $k \geq 0$ and consider iteration $k+1$ of the loop. The iteration first defines $v = d_{\min}[a] h_\theta^{-1}\left([a]^{-1} f_{\text{cyc}}^{(k)} + [a]^{-1} f_{\text{cut}}\right)$ on line 6. Then on line 7,

$$w = \underset{w \in \mathbb{R}^n}{\text{argmin}} \left\{||B[a]B^\top w - Bv||_2\right\} = \left(B[a]B^\top\right)^{\dagger} Bv$$

and line 8 defines

$$\Delta f_{\text{cyc}} = v - [a]B^\top w = \left(I_m - [a]B^\top \left(B[a]B^\top\right)^{\dagger}\right) v = Pv$$

Finally, on line 9,

$$f_{\text{cyc}}^{(k+1)} = f_{\text{cyc}}^{(k)} - Pv = f_{\text{cyc}}^{(k)} - d_{\min} P[a] h_\theta^{-1}\left([a]^{-1} f_{\text{cyc}}^{(k)} + [a]^{-1} f_{\text{cut}}\right)$$

A simple inductive argument shows that $f_{\text{cyc}}^{(k)} \in \ker(B)$. The base case $f_{\text{cyc}}^{(0)} = \mathbb{0}_m$ is trivial, for all $k' \geq 0$, line 9 ensures that $f_{\text{cyc}}^{(k'+1)} \in \ker(B)$ so long as $f_{\text{cyc}}^{(k')} \in \ker(B)$. Hence $f_{\text{cyc}}^{(k)} = P f_{\text{cyc}}^{(k)}$, and we conclude that

$$f_{\text{cyc}}^{(k+1)} = P\left(f_{\text{cyc}}^{(k)} - d_{\min}[a] h_\theta^{-1}\left([a]^{-1} f_{\text{cyc}}^{(k)} + [a]^{-1} f_{\text{cut}}\right)\right) = T(f_{\text{cyc}}^{(k)})$$

To prove statement 2, recall from Theorem 2.2 that $\mathrm{Lip}(T) \leq 1 - d_{\max}^{-1} d_{\min}$, which (together with statement 1) implies that, for all $k \geq 0$,

$$\begin{aligned}
||f_{\mathrm{cyc}}^{(k+1)} - f_{\mathrm{cyc}}^{(k)}||_{2,[a]^{-1}} &\leq \left(1 - \frac{d_{\min}}{d_{\max}}\right)^k ||f_{\mathrm{cyc}}^{(1)} - f_{\mathrm{cyc}}^{(0)}||_{2,[a]^{-1}} \\
&= d_{\min} \left(1 - \frac{d_{\min}}{d_{\max}}\right)^k ||P[a]h_\theta^{-1}\left([a]^{-1}B^\dagger u\right)||_{2,[a]^{-1}} \\
&= d_{\min} \left(1 - \frac{d_{\min}}{d_{\max}}\right)^k \rho
\end{aligned}$$

The algorithm terminates after iteration k if and only if $||f_{\mathrm{cyc}}^{(k)} - f_{\mathrm{cyc}}^{(k-1)}||_{2,[a]^{-\frac{1}{2}}} \leq \epsilon$, so the algorithm will have terminated after k^* iterations if

$$d_{\min} \left(1 - \frac{d_{\min}}{d_{\max}}\right)^{k^*-1} \rho \leq \epsilon$$

which is equivalent to

$$k^* \geq 1 + \frac{\log\left(d_{\min}^{-1}\rho^{-1}\epsilon\right)}{\log\left(1 - \frac{d_{\min}}{d_{\max}}\right)}$$

Finally, to prove statement 3, note that the algorithm terminates after iteration k as soon as

$$||f_{\mathrm{cyc}}^{(k)} - f_{\mathrm{cyc}}^{(k-1)}||_{2,[a]^{-1}} \leq \epsilon$$

If f_{cyc} is the true fixed point of T, then using a general property of contraction mappings,

$$\begin{aligned}
||f_{\mathrm{cyc}}^{(k)} - f_{\mathrm{cyc}}||_{2,[a]^{-1}} &\leq \frac{\mathrm{Lip}(T)}{1 - \mathrm{Lip}(T)} ||f_{\mathrm{cyc}}^{(k)} - f_{\mathrm{cyc}}^{(k-1)}||_{2,[a]^{-1}} \\
&\leq \left(\frac{d_{\max} - d_{\min}}{d_{\min}}\right)\epsilon
\end{aligned}$$

Therefore, the vector f returned by the algorithm satisfies

$$||f - \mathrm{FN}_{h,\theta}(G,u)||_{2,[a]^{-1}} = ||f_{\mathrm{cyc}}^{(k)} - f_{\mathrm{cyc}}||_{2,[a]^{-1}} \leq \left(\frac{d_{\max} - d_{\min}}{d_{\min}}\right)\epsilon$$

A.3 Proof of Theorem 2.4

Let $v = [a]h_\theta^{-1}([a]^{-1}f_{\mathrm{cyc}} + [a]^{-1}B^\dagger u)$. From Theorem 2.2, we can write $f = f_{\mathrm{cyc}} + B^\dagger u$, where f_{cyc} is the unique fixed point of T. Therefore $\frac{df}{dw} = \frac{df_{\mathrm{cyc}}}{dw} + B^\dagger \frac{du}{dw}$, so the remainder of the proof is to show that $\frac{df_{\mathrm{cyc}}}{dw} = \mathrm{FN}_{g,\cdot}(G, \mathbb{0}_n)$.

Since $f_{\mathrm{cyc}} = T(f_{\mathrm{cyc}})$, and $Pf_{\mathrm{cyc}} = f_{\mathrm{cyc}}$, we have

$$f_{\mathrm{cyc}} = P\left(f_{\mathrm{cyc}} - d_{\min}v\right) = f_{\mathrm{cyc}} - d_{\min}Pv$$

so an equivalent characterization of f_{cyc} is the unique solution to the equations

$$\begin{aligned}
Bf_{\mathrm{cyc}} &= \mathbb{0}_n \\
Pv &= \mathbb{0}_m
\end{aligned}$$

Since

$$\frac{dv}{dw} = \frac{\partial v}{\partial w} + \frac{\partial v}{\partial f_{\mathrm{cyc}}}\frac{df_{\mathrm{cyc}}}{dw} = \frac{\partial v}{\partial w} + \mathcal{D}\frac{df_{\mathrm{cyc}}}{dw}$$

then differentiating and factoring out $[a]$, we obtain

$$\begin{aligned}
B\frac{df_{\mathrm{cyc}}}{dw} &= \mathbb{0}_n \\
P[a]\left([a]^{-1}\frac{\partial v}{\partial w} + [a]^{-1}\mathcal{D}\frac{df_{\mathrm{cyc}}}{dw}\right) &= \mathbb{0}_m
\end{aligned}$$

Since $\ker(P[a]) = \mathrm{Img}(B^\top)$, there exists $x \in \mathbb{R}^n$ such that

$$[a]^{-1}\frac{\partial v}{\partial w} + [a]^{-1}\mathcal{D}\frac{df_{\text{cyc}}}{dw} = B^\top x$$

which we can re-write as

$$\frac{df_{\text{cyc}}}{dw} = [a]\mathcal{D}^{-1}\left(B^\top x - [a]^{-1}\frac{\partial v}{\partial w}\right) = [a]g(B^\top x)$$

Hence $\frac{df_{\text{cyc}}}{dw}$ is the solution to

$$B\frac{df_{\text{cyc}}}{dw} = \mathbb{0}_n \tag{19}$$

$$\frac{df_{\text{cyc}}}{dw} = [a]g(B^\top x) \tag{20}$$

which is identical to (3)–(4) with $\frac{df_{\text{cyc}}}{dw}$ in place of f, $\mathbb{0}_n$ in place of u, and g in place of h_θ. Furthermore, g respects the same $d_{\min}, d_{\max}$ derivative constraints as h_θ, since for each $e \in \mathcal{E}$,

$$g'_e(\eta_e) = \frac{1}{\mathcal{D}_{ee}} = \left.\frac{dh_\theta(y_e)}{dy_e}\right|_{y_e = a_e^{-1}f_e} \in [d_{\min}, d_{\max}]$$

It follows that $\frac{df_{\text{cyc}}}{dw}$ is the output of the implicit flow network with flow functions g and parameters $d_{\min}, d_{\max}$, evaluated on the original graph G and nodal demands $\mathbb{0}_n$.

A.4 Proof of Theorem 3.1

Since h_θ^{-1} is increasing, the optimization problem in (14) has a convex cost function with linear constraints, so the KKT conditions are necessary and sufficient. Letting $x \in \mathbb{R}^m$ be a vector of Lagrange multipliers, the Lagrangian is

$$\mathcal{L} = \sum_{e\in\mathcal{E}} \int_0^{f_e} h_\theta^{-1}(a_e^{-1}z)\, dz - x^\top (Bf - u)$$

leading to the stationarity condition

$$\mathbb{0}_m^\top = \frac{\partial \mathcal{L}}{\partial f} = h_\theta^{-1}(f^\top [a]^{-1}) - x^\top B$$

which is equivalent to (4). Additionally, the primal constraint $Bf = u$ is equivalent to (3), so the minimizer of the optimization problem is identical to the output of the IFN.

A.5 Proof of Theorem 4.2

Due to (L3), it is clear that the derivative bounds (16) hold if and only if

$$\left|\frac{\mathrm{dN}_0(x,\theta)}{\mathrm{d}x}\right| \le 1, \qquad \forall x \in \mathbb{R} \tag{21}$$

For all $x, x' \in \mathbb{R}$, by Hölder's inequality,

$$\begin{aligned}|\mathrm{N}_0(x,\theta) - \mathrm{N}_0(x',\theta)| &= \left|\bar{c}^\top(\theta)\left(\sigma(ax+b) - \sigma(ax'+b)\right)\right| \\ &\le ||\bar{c}(\theta)||_p \, ||\sigma(ax+b) - \sigma(ax'+b)||_q\end{aligned}$$

Since σ is non-expansive, its Lipschitz constant with respect to the q-norm is

$$\mathrm{Lip}(\sigma) = \sup_{\eta\in\mathbb{R}^k} \left|\left|\frac{\partial\sigma(\eta)}{\partial\eta}\right|\right|_q = \sup_{\eta_0\in\mathbb{R}} |\sigma'(\eta_0)| \le 1$$

and thus

$$||\sigma(ax+b) - \sigma(ax'+b)||_q \le ||a(x-x')||_q \le ||a||_q |x - x'|$$

Test Case	MATPOWER Case Name	$\lvert\mathcal{V}\rvert$	$\lvert\mathcal{E}\rvert$
IEEE-57	`case57`	57	135
IEEE-118	`case118`	118	297
IEEE-145	`case145`	145	567
IEEE-300	`case300`	300	709
ACTIVSg200	`case_ACTIVSg200`	200	445
ACTIVSg500	`case_ACTIVSg500`	500	1084

Table 2: MATPOWER test case details.

Furthermore, by (L1),

$$\begin{aligned}||\bar{c}(\theta)||_p||a||_q &= \left(1 - \frac{(||c||_p||a||_q - 1)_+}{||c||_p||a||_q}\right)||c||_p||a||_q \\ &= ||c||_p||a||_q - (||c||_p||a||_q - 1)_+ \\ &= \min\{1, ||c||_p||a||_q\}\end{aligned}$$

so that

$$|\mathrm{N}_0(x,\theta) - \mathrm{N}_0(x',\theta)| \leq \min\{1, ||c||_p||a||_q\}\,|x - x'| \leq |x - x'|$$

for all x, x'. Hence (21) is satisfied.

B Experiment Details

B.1 AC Power Datasets

We created datasets from 6 AC power network test cases. Each dataset that we created represents a snapshot of an AC power network in its steady state, consisting of four components: the network topology (as an oriented, undirected graph), four attributes on each edge (voltage magnitude at the two incident nodes, series reactance, and tap ratio), the net power injection at each node, and the active power flow through each branch.

Original Data We generated our datasets using MATPOWER, an open-source toolbox for power system simulation in MATLAB [36]. The toolbox includes many standard test cases, which contain a network topology and tables of electrical and economic parameters for each bus (node), branch (edge), and generator. We selected 6 test cases, listed in Table 2. The raw data files for these test cases are available from the MATPOWER source[3], and details on the test case file format are contained in Appendix B of the user manual[4].

Data Generation After loading each test case into MATPOWER, we performed the following two modifications of the network parameters:

1. We set branch resistances (column 3 in the branch data table) to zero, so that transmission lines in the system are lossless. This step was necessary because IFN is limited to undirected graphs, while lossy lines are more appropriately modeled with a pair of directed edges, since the power injected at one endpoint does not equal the power withdrawn from the other endpoint. Fortunately, branch resistances are typically small before this modification.
2. We replaced any negative series reactances (column 4 in the branch data table) with a positive value, chosen as the median of the positive series reactances in the same network. We performed this modification because negative series reactances results in *decreasing* constitutive relationships on the corresponding edges, whereas IFN assumes that the constitutive relationship is increasing. This modification only affected two networks: IEEE-145, in which 24 (4.2%) of the branches were assigned a series reactance of 0.2306; and IEEE-300, in which 1 (0.1%) of the branches was assigned a series reactance of 0.059.

We then computed the resulting power flows using the `runpf` function and recorded the results.

[3] https://github.com/MATPOWER/matpower/tree/master/data

[4] https://matpower.org/docs/MATPOWER-manual.pdf

Test Case	$\lvert\mathcal{V}\rvert$	$\lvert\mathcal{E}\rvert$
Fairfield	111	125
Bellingham	121	162
Harrisburg	261	286

Table 3: Water distribution network details.

Pre-Processing Finally, we converted the results from the MATPOWER simulation into a PyTorch Geometric data object, with the following attributes:

- `edge_index`, the edge index tensor, containing the topology from the test case.
- `x`, a tensor of net active power injections at each node, which has the property that $\mathbb{1}_n^\top x = 0$. (This tensor is identical to the supply / demand vector u in the paper.)
- `edge_attr`, a tensor of four relevant attributes for each edge: the voltage magnitudes at the two incident nodes, the series reactance, and the tap ratio.
- `f_true`, the tensor of active power flows on each edge simulated by MATPOWER.

The net active power injections at each node are computed according to

$$u_i = \mathrm{PG}_i - \mathrm{PD}_i - \mathrm{GS}_i \mathrm{VM}_i^2$$

where PG_i is active power generated at i, PD_i is active power demanded, GS_i is shunt conductance, and VM_i is the voltage magnitude.

B.2 Water Distribution Dataset

We created 3 datasets representing snapshots of municipal water distribution networks in their steady state, consisting of four components: the network topology (as an oriented, undirected graph), weights for each edge, the net inflow rates at each node, and the flow rate through each pipe.

Original Data Each of the datasets is based on a network from the ASCE Task Committee on Research Databases for Water Distribution Systems database [37]. Networks in this database contain a distribution network topology and tables of hydraulic parameters and operating characteristics for each node, pipe (edge), pump, reservoir, and storage tank in the network. We selected 3 networks, listed in Table 3 and plotted in Figure 4. The raw data files are available online[5].

Data Generation and Preprocessing We loaded each network INP file into WNTR and ran the WNTR simulator with a hydraulic accuracy of 10^{-8}. We then converted the results into a PyTorch Geometric data object, with the following attributes:

- `edge_index`, the edge index tensor, containing the topology from the test case.
- `x`, a tensor of net inflows at each node, which has the property that $\mathbb{1}_n^\top x = 0$.
- `edge_attr`, a tensor of three relevant attributes for each edge: the pipe length, pipe diameter, and pipe roughness coefficient.
- `f_true`, the tensor of flow rates through each pipe simulated by WNTR.

Edge weights are computed according to the formula

$$a_e = (0.27855) C_e D_e^{2.63} L_e^{-0.54} \tag{22}$$

where C_e is the roughness coefficient (unitless), D_e is the diameter (meters), and L_e is the pipe length (meters) [6].

[5] http://www.uky.edu/WDST/index.html

[6] https://wntr.readthedocs.io/en/latest/hydraulics.html

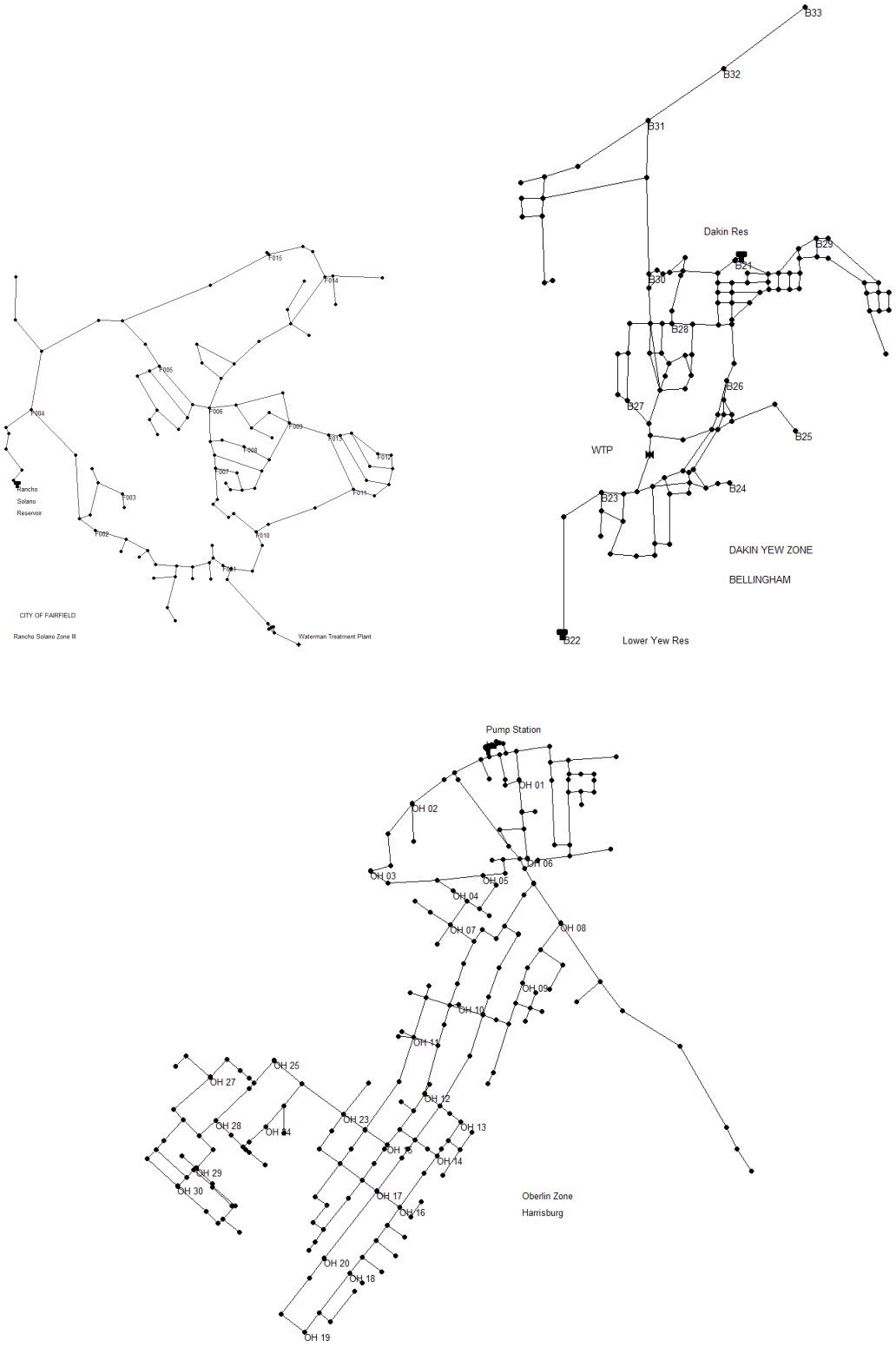

Figure 4: Network maps of the three water distribution systems: Fairfield (upper left), Bellingham (upper right), and Harrisburg (bottom).

B.3 Details on IFN

Our IFN implementation uses Algorithm 1 to compute the layer's forward pass. We set the maximum number of iterations in this algorithm to 100, with a tolerance of $\epsilon = 10^{-2}$ for power and $\epsilon = 10^{-4}$ for water. With the release of PyTorch 1.11.0, the `torch.linalg.lstsq` method[7] now supports automatic differentiation, allowing PyTorch to automatically backpropagate through the Algorithm 1 iterations, instead of using Theorem 2.4. We found that Algorithm 1 terminated with a small enough number of iterations that automatic differentiation was faster, so we opted to use this rather than the method from Theorem 2.4. We trained the IFN models to minimize the RMSE loss function by minimizing the RMSE loss function

$$\ell_{\text{rmse}} = \sqrt{\frac{1}{|\mathcal{E}_l|} \sum_{e \in \mathcal{E}} \left(f_e - \text{FN}_{h,\theta}(G, u)_e\right)^2}$$

B.4 Details on Baselines

We implemented all of the baselines by adapting Silva's code[8] from [4], refactoring some utility functions to decrease runtime. Following [4], we perform the following two data normalization steps:

1. negative flows are converted into positive flows by flipping the orientation of the corresponding edges and replacing the entries of `f_true` with their absolute value, and
2. flows are proportionally normalized to the range $[0, 1]$ within each network.

After training with the normalized flows and computing the missing flow predictions, the predictions are denormalized before computing the testing RMSE.

Div The minimizing divergence baseline from [3] has a single hyperparameter, λ, from the regularization term $\lambda^2 ||f||_2^2$ in the loss function. We set $\lambda = 0.1$ for all networks and fractions of labeled edges by hand-tuning the parameter to the proper order of magnitude.

Bilevel Baselines All three of the bilevel baselines (Bil-MLP, Bil-GCN, and Bil-True) have several hyperparameters related to the bilevel optimization algorithm. For most of these parameters, we use the same settings as [4]: the number of iterations for the inner optimization problem is 300 during training and 3000 during evaluation, and the number of k-fold cross validation folds is 10; however, we increased the number of iterations of the outer optimization problem from 10 to 100, with an early stopping interval of 10, to ensure that the outer optimization problem was given sufficient time to converge. As with [4], we used a 2-layer MLP and GCN in Bil-MLP and Bil-GCN, respectively, but we increased the size of the hidden layer to 64.

Bil-True Like IFN, the baselines Bil-MLP and Bil-GCN train a model to predict edge weights from side information (if we interpret $\mathcal{Q}$ as a diagonal matrix of edge weights). We devised Bil-True as a third baseline to use the "ground-truth edge weights" instead of training a model. For water experiments, these ground-truth edge weights are given by (22). For the power experiments, we compute these edges weights from the AC active power flow equation: in a lossless AC power grid, active power flows f_{ij} on each edge $\{i, j\} \in \mathcal{E}$ are given by

$$f_{ij} = \frac{v_i v_j}{x_{ij}\tau_{ij}} \sin(\theta_i - \theta_j) \approx \frac{v_i v_j}{x_{ij}\tau_{ij}} (\theta_i - \theta_j) \tag{23}$$

where v_i, v_j are the voltage magnitudes on incident nodes, x_{ij} is the series reactance, τ_{ij} is the tap ratio, and θ_i, θ_j are the incident voltage angles. Since (23) is the constitutive relationship for AC power networks, examining its linear approximation in light of (15) suggests using $x_{ij}\tau_{ij}/v_i v_j$ as the regularizer weight on f_{ij}.

B.5 Details on Training

We trained all models in a Google Colab notebook, using the Adam optimizer. We used an initial learning rate of 0.01, which we found to have good performance for all of the models. Training was terminated when the training loss had not decreased for 10 epochs.

[7] https://pytorch.org/docs/stable/generated/torch.linalg.lstsq.html
[8] https://openreview.net/forum?id=l0V53bErniB